

Radiative Lifetime of Excitons in Carbon Nanotubes

Vasili Perebeinos*, J. Tersoff, and Phaedon Avouris

IBM Research Division, T. J. Watson Research Center, Yorktown Heights, New York 10598

(Dated: August 20, 2018)

We calculate the radiative lifetime and energy bandstructure of excitons in semiconducting carbon nanotubes, within a tight-binding approach. In the limit of rapid interband thermalization, the radiative decay rate is maximized at intermediate temperatures, decreasing at low temperature because the lowest-energy excitons are optically forbidden. The intrinsic phonons cannot scatter excitons between optically active and forbidden bands, so sample-dependent extrinsic effects that break the symmetries can play a central role. We calculate the diameter-dependent energy splittings between singlet and triplet excitons of different symmetries, and the resulting dependence of radiative lifetime on temperature and tube diameter.

PACS numbers: 78.67.Ch, 73.22.Lp

The potential usefulness of carbon nanotubes as an optical material depends sensitively on the luminescence efficiency, which in turn depends on the radiative lifetime. Yet while the optical properties of nanotubes have been studied intensely [1, 2, 3, 4, 5, 6, 7, 8, 9, 10, 11, 12, 13], little is known about the radiative lifetime, and its dependence on temperature and tube diameter. It is by now well recognized that optical absorption and emission in nanotubes are dominated by excitons [10, 12, 13], posing an additional challenge.

Here we calculate the exciton bandstructure and radiative lifetime in carbon nanotubes. When interband thermalization is efficient, we find that the lifetime has a minimum at *intermediate* temperatures, with optical recombination becoming slower both at very low and very high temperature. This unusual behavior occurs because the lowest-energy excitons are optically forbidden by symmetry [12, 14]. We report the energy differences between singlet and triplet excitons of different symmetries, for a range of nanotube diameters. We also present the resulting temperature dependences of the radiative lifetime. Both the energies and temperature dependences are well described by simple scaling formulas. The optically allowed band has a non-analytic dispersion due to exchange, while the other bands have a mass enhancement of $\sim 50\%$ over free electron-hole pairs.

We find that symmetry plays a special role in this system. For photoluminescence of an ideal nanotube (and neglecting spin-orbit coupling), phonons cannot scatter excitons into the optically forbidden low-energy states, so optical emission is very efficient. However, extrinsic effects that break the ideal symmetry can qualitatively change the behavior, especially at low temperature. Such effects can also lead to multiple peaks in emission spectra with characteristic temperature dependence, perhaps explaining experimental observations [15, 16].

The quantum efficiency η of light emission corresponds to the fraction of excitons decaying by radiative channels: $\eta = \tau_{nr}/(\tau_r + \tau_{nr})$, where τ_r and τ_{nr} are the radiative and nonradiative lifetimes. The total decay rate (i.e. in-

verse lifetime) is $\tau_{tot}^{-1} = \tau_r^{-1} + \tau_{nr}^{-1}$. It has been measured [17, 18, 19, 20, 21], and environmental effects have been recently published [22]. But only one measurement of radiative lifetime has been reported [20].

A photoexcited state has total momentum $q = q(\text{photon})$, hereafter approximated as $q = 0$. It is rapidly scattered by phonons into a different state with $q \neq 0$ [13], and cannot decay directly. Therefore what is relevant is not the lifetime of a specific excitonic state, but rather the lifetime of an exciton as it scatters from one state to another. If thermalization is inefficient, then the lifetime depends on the details of the excitation process and subsequent scattering pathways.

We therefore focus first on the case where the exciton thermalizes on a timescale much shorter than the decay time [17, 18, 19, 20, 21]. Then at low excitation density there are well-defined (thermally averaged) radiative and non-radiative lifetimes. The radiative decay rate (i.e. inverse radiative lifetime) is [23]

$$\tau_r^{-1} = \frac{1}{Z(T)} \sum_{\nu} \tau_{\nu}^{-1} \exp\left(\frac{-E_{\nu}}{k_B T}\right), \quad (1)$$

and a similar formula applies for nonradiative decay. The index $\nu = (q, j, S, \sigma)$ may include summation over exciton wavevector q , angular momentum j (i.e. discrete wavevector around the tube), spin index σ (labelling singlet and triplet states), and exciton state S (labelling the bound and continuum states for a given q and σ); or it may be restricted to those states accessible by symmetry-allowed scattering mechanisms, as discussed below. The partition function is $Z(T) = \sum_{\nu} \exp(-E_{\nu}/k_B T)$, summed over the same range of ν . The radiative decay rate for each excitonic state is [25]

$$\tau_{\nu}^{-1} = \frac{n e^2 E_{\nu}^2 f_{\nu}}{2 \pi \epsilon_0 m_e \hbar^2 c^3} \quad (2)$$

where n is the refractive index (hereafter $n = 1.4$). We calculate the exciton energies E_{ν} and the corresponding oscillator strengths f_{ν} using a tight-binding Hamiltonian [26] with $t = 3.0$ eV, and solving the Bethe-Salpeter

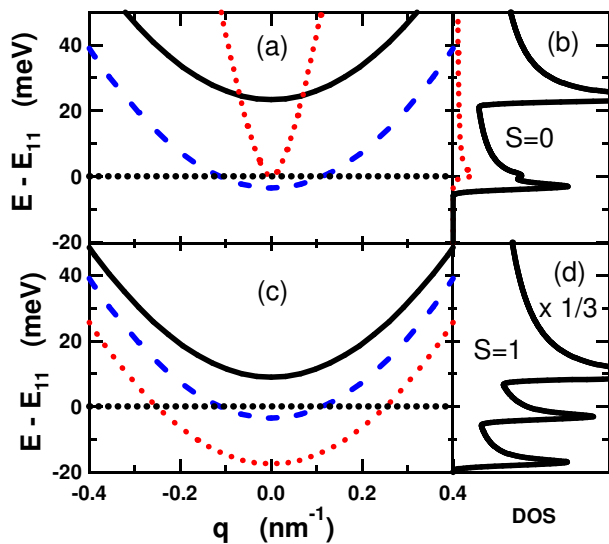


FIG. 1: Four lowest-energy exciton bands of a (19,0) nanotube ($d = 1.5$ nm) embedded in medium having $\epsilon = 2$ [12], for (a) singlet and (c) triplet spin states. The black solid curves are doubly degenerate exciton bands having nonzero angular momentum. The blue dashed curves are even parity (dipole forbidden) exciton bands having zero angular momentum. The red dotted curves are the odd parity (dipole allowed) exciton bands having zero angular momentum. The density of states for (b) singlet and (d) triplet states are shown by the black curves. The red dotted curve in (b) shows the partial density of states for dipole allowed singlet exciton. The change in scale of $1/3$ in (d) is for triplet degeneracy.

Equation (BSE) [27], as in Refs. [12, 13], taking the surrounding medium to have dielectric constant $\epsilon = 2$.

In an idealized picture, one exciton can capture much of the spectral weight of the entire nanotubes [28]. But in reality, phonon scattering limits the exciton coherence to a finite length scale, and spreads the oscillator strength of the exciton over a finite linewidth [23]. As long as the linewidth is substantially less than $k_B T$ [15], we obtain good accuracy from Eq. (1) without including this linewidth explicitly.

For a single 1D exciton band with parabolic dispersion, the temperature dependence of the radiative lifetime [Eq. (1)] is $\tau_r \propto T^{1/2}$ [24]. However, as shown in Fig. 1, here there are several low-lying bands, with the lowest being optically forbidden [12, 14]. Thus it is important to understand the exciton energies and symmetries in some detail.

The conduction and valence bands in carbon nanotubes are doubly degenerate. For free electron-hole pairs, this gives four distinct but degenerate pair excitations. In excitons, the Coulomb interaction partially lifts the fourfold degeneracy. The dispersions of the four lowest-energy singlet excitons are shown in Fig. 1a. The lowest-energy exciton at $q = 0$ has zero angular momentum and even parity, so it is dipole forbidden [12].

The second exciton also has zero angular momentum, but with odd parity, and it gives rise to the E_{11} optical transition. The next two excitons at $q = 0$ lie above the E_{11} transition energy. They are degenerate, with positive and negative angular momentum, and are therefore optically forbidden; but they can be observed in phonon-assisted absorption [13].

The optically forbidden excitons all have similar effective masses, $m^* \sim 1.5(m_e + m_h)$, where $m_e = m_h$ is the effective mass of an electron or hole. The 50% mass enhancement is roughly independent of tube diameter.

In contrast, the dispersion of the optically active exciton is extremely steep and non-parabolic, going as $q^2 \ln |q|$. A similar logarithmic contribution to the electron self energy was found in 2D graphene [29]. This anomalous dispersion occurs because of the exchange energy, which for the other bands is either zero by symmetry, or is a smooth function of q .

In photoluminescence experiments, excitons are optically pumped into a singlet spin state of odd parity. For an ideal nanotube (and neglecting spin-orbit coupling), we find that phonons cannot scatter an exciton between states of different parity or different spin. Therefore the exciton will thermalize within the odd-parity spin-singlet bands (solid black and dotted red in Fig. 1a), and the sums in Eq. (1) and $Z(T)$ need to be restricted accordingly. The resulting behavior is shown in Fig. 2a. At low temperature, the behavior is well approximated as $\tau_r \propto T^{0.55}$, slightly different than $T^{1/2}$ dependence [24] due to the nonparabolic dispersion. At higher temperature, the behavior is quite different, reflecting the contribution of the higher-energy bands to $Z(T)$; it is well approximated by $\tau_r \propto T^{3/2}$.

This ideal picture, while appealing in its simplicity, may not be directly applicable to experiment. There are many effects that tend to break the symmetries of the perfect nanotube: coupling to the environment, structural distortions, finite size and associated end effects, and the presence of defects or impurities. These effects allow scattering and thermalization between bands of different parity and/or different spin. This tends to suppress luminescence at low temperature, because excitons thermalize to a low-energy band that is optically forbidden. At the same time, luminescence is suppressed at high temperature because a larger range of q becomes thermally accessible. These effects enter via $Z(T)$ in Eq. (1).

Fig. 2b shows the case of scattering and thermalization between different parity, but not between different spin states; and Fig. 2c shows the case of thermalization among states of all parities and spins. We find that the temperature dependence of τ_r is very similar in all cases where thermalization includes a low-energy forbidden band, except for an overall scaling of τ and T . This is shown in Fig. 2e, where all the curves in Figs. 2b-c collapse nearly to a single scaled curve. A simple in-

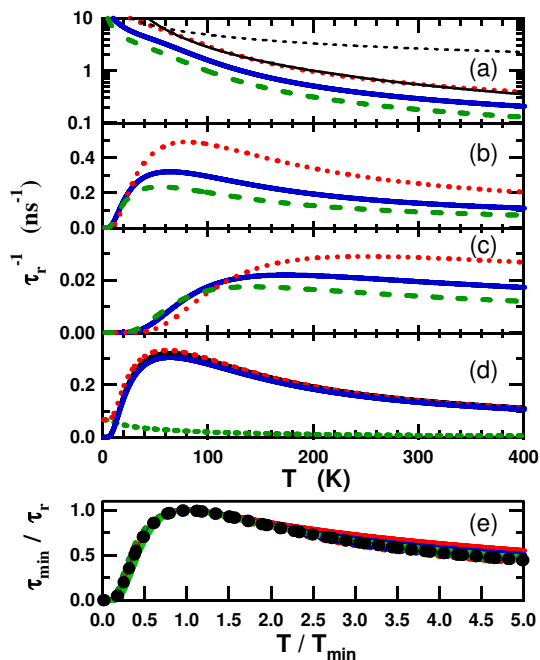


FIG. 2: Exciton radiative decay rate τ_r^{-1} [Eq. (1)] as a function of temperature, in a medium having $\epsilon = 2$ [12]. Curves in (a-c) are for zig-zag tubes with diameters 1.0 nm (dotted red), 1.5 nm (solid blue), and 2.0 nm (dashed green). Fine dotted black line in (a) shows fit of 1.0 nm curve to $T^{-0.55}$ at low T and $T^{-3/2}$ at high T . In (a) only singlet states of odd parity are included; (b) assumes thermalization between singlet states of even and odd parity; and (c) assumes thermalization between both singlet and triplet states of both parities. Effect of symmetry mixing is illustrated in (d) for 1.5 nm tube as in (b), but including a 5% mixing of spectral weight into the even-parity band. Solid blue curve shows decay rate from main E_{11} peak, which is only very slightly reduced relative to (b). Dotted green line is contribution from nominally forbidden exciton 3.5 meV lower in energy. Dashed red line is total radiative decay rate. Temperature dependence of dotted green curve depends on q -dependence assumed for mixing. (e) Scaled radiative lifetimes for all six curves from (b) and (c). The empirical scaling formula Eq. (3) is shown by a dotted black-on-white curve.

interpolation formula can describe this scaled temperature dependence:

$$\frac{\tau_r}{\tau_{\min}} = \frac{T}{T_{\min}} \exp\left(\frac{T_{\min} - T}{T}\right). \quad (3)$$

The diameter dependence of τ_{\min} and T_{\min} are shown in Fig. 3a and 3b respectively, along with the best fits to the simple empirical relations:

$$\tau_{\min} \approx \tau_0 + \alpha d, \quad T_{\min} \approx \frac{\beta}{d}. \quad (4)$$

For small-diameter (large-bandgap) tubes, the maximum radiative decay rate τ_{\min}^{-1} is higher, and this maximum rate occurs closer to room temperature.

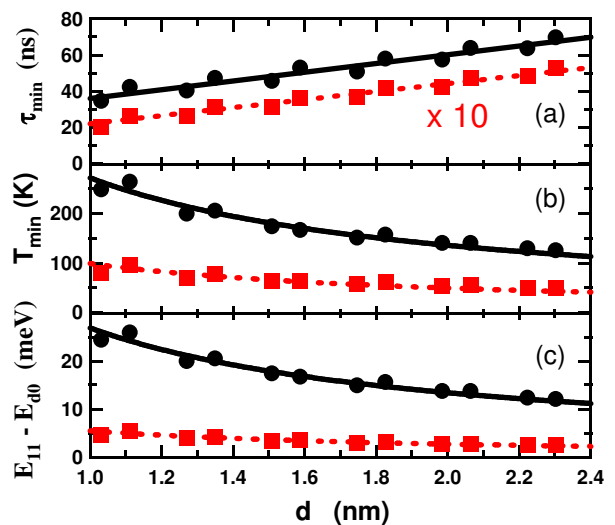


FIG. 3: Diameter dependence in zig-zag semiconducting nanotubes of (a) the minimum radiative lifetime, (b) the corresponding temperature, and (c) the energy splitting between the optically active exciton and the lowest energy exciton, along with best fits to Eq. (4–5). Black circles are the results, when both triplet and singlet states are included; red squares are with only singlet excitons included. Thus the black circles in (c) correspond to the singlet-triplet splitting of the dipole-allowed states at $q = 0$. Solid curves are interpolation formulas, Eq. (4) and Eq. (5). Note the $\times 10$ multiplication factor for the red squares in (a).

T_{\min} is approximately proportional to the energy difference between the optically active exciton (E_{11}), and the lowest-energy exciton that participates in thermalization (E_{d0}). This difference $E_{11} - E_{d0}$ is shown in Fig. 3c. The singlet-triplet exchange splitting of the dipole-allowed exciton, as well as the even-odd parity splitting of the singlet exciton, are both inversely proportional to the tube diameter:

$$E_{11} - E_{d0} \approx \frac{\gamma}{d}. \quad (5)$$

The singlet-triplet splitting is expected to scale with the size of the exciton, which is proportional to the tube diameter [12]. The splitting between the even and odd parity excitons is a factor of five smaller than the singlet-triplet exchange splitting.

In Fig. 3, τ_{\min} , T_{\min} , and $E_{11} - E_{d0}$ all exhibit alternations in the diameter dependence, due to the systematic difference between tubes having $\text{mod}(n-m,3)=1$ or 2. While only zigzag tubes are shown here, we find very similar diameter dependence for other chiralities.

Equations (3–4) provide an estimate of the temperature dependent radiative lifetime in this tube diameter range, whenever thermalization with optically forbidden symmetries occurs. The best-fit values of the three parameters are: $\tau_0 = 12$ ns, $\alpha = 24$ ns/nm, and $\beta = 272$ K-nm, if both singlet and triplet excitons contribute to $Z(T)$; and $\tau_0 = 0$ ns, $\alpha = 2.2$ ns/nm, and $\beta = 99$ K-nm

if only singlet excitons contribute. The singlet-triplet exchange splitting and the even-odd parity splitting at $q = 0$ are given by Eq. (5), with $\gamma = 27$ meV-nm and $\gamma = 5.5$ meV-nm respectively.

At sufficiently low temperature, additional complications arise. Thermalization by acoustic phonons becomes less effective [30], so it is less likely that this equilibrium picture will apply. Also, even weak disorder from environmental interactions would lead to localization of band-edge excitons. Because localized excitons that are close in energy can be well separated spatially, they typically are not in thermal equilibrium at low T . This will give a finite linewidth determined by the strength of the disorder, even at $T = 0$.

Interband scattering necessarily implies some mixing of the bands; so in the cases of inter-symmetry scattering (Fig. 2b-c), the optically forbidden bands are no longer strictly forbidden. Rather, there is some small but finite radiative decay rate τ_{ν}^{-1} associated with every participating band. For thermalization at sufficiently low T , only the lowest-energy of these bands will have significant occupancy. Then the emission from this “nearly-forbidden” band, however small, will dominate over thermal excitation into the optically allowed band.

In this case, the emission spectrum (not shown) has two peaks, one from the optically allowed band, and one at lower energy from the nominally forbidden band. The latter may be negligibly weak at high temperature, but becomes dominant at sufficiently low temperature (as long as thermalization occurs before decay). We illustrate this in Fig. 2d, for one particular model of the mixing.

Thus the behavior is sensitive to deviations from ideality, which will in general vary among different experiments. Single-tube spectroscopy at low temperature provides a powerful diagnostic of such extrinsic effects. Any distinct emission peak at lower energy than the main peak implies some symmetry breaking. If the peaks do not correspond to the few distinct bands of Fig. 1, they are likely to correspond to excitons that are localized (e.g. at defects or deformations). A finite peak width as $T \rightarrow 0$ suggests disorder (along with the expected breakdown of thermalization). Recent measurements are suggestive in showing multiple peaks, with spectral weight shifting from high- to low-energy peaks with decreasing temperature [15, 16].

-
- [*] Electronic address: vperebe@us.ibm.com
- [1] Z. M. Li *et al.*, Phys. Rev. Lett. **87**, 127401 (2003).
- [2] M. J. O’Connell *et al.*, Science, **297**, 593 (2002).
- [3] S. M. Bachilo, M. S. Strano, C. Kittrell, R. H. Hauge, R. E. Smalley, R. B. Weisman, Science, **298**, 2361 (2002).
- [4] A. Hagen and T. Hertel, Nano Lett. **3**, 383 (2003)
- [5] S. Lebedkin, F. Hennrich, T. Skipa, and M. M. Kappes, J. Phys. Chem. B **107**, 1949 (2003).
- [6] J. Lefebvre, Y. Homma, and P. Finnie, Phys. Rev. Lett. **90**, 217401 (2003)
- [7] T. Ando, J. Phys. Soc. Japan **66**, 1066 (1996).
- [8] T. G. Pedersen, Phys. Rev. B **67**, 073401 (2003).
- [9] C.L. Kane and E. J. Mele, Phys. Rev. Lett. **90**, 207401 (2003).
- [10] C. D. Spataru, S. Ismail-Beigi, L. X. Benedict, and S. G. Louie, Phys. Rev. Lett. **92**, 077402 (2004); Appl. Phys. A **78**, 1129 (2004).
- [11] E. Chang, G. Bussi, A. Ruini, and E. Molinari, Phys. Rev. Lett. **92**, 196401 (2004).
- [12] V. Perebeinos, J. Tersoff, Ph. Avouris, Phys. Rev. Lett. **92**, 257402 (2004).
- [13] V. Perebeinos, J. Tersoff, Ph. Avouris, Phys. Rev. Lett. **94**, 027402 (2005).
- [14] H. Zhao and S. Mazumdar, Phys. Rev. Lett. **93**, 157402 (2004) identify a key issue, that low-energy forbidden states may reduce the efficiency. However, their exciton degeneracies and relative energies are different than found here, perhaps due to their particular finite molecular system.
- [15] J. Lefebvre, P. Finnie, and Y. Homma, Phys. Rev. B **70**, 045419 (2004); and private communication.
- [16] A. Hagen, M. Steiner, M. B. Raschke, C. Lienau, T. Hertel, H. Qian, A. J. Meixner, A. Hartschuh, (unpublished).
- [17] Y.-Z. Ma *et al.*, J. Chem. Phys. **120**, 3368 (2004).
- [18] G. N. Ostojic *et al.*, Phys. Rev. Lett. **92**, 117402 (2004).
- [19] S. Reich, M. Dworzak, A. Hoffmann, and C. Thomsen, and M. S. Strano, Phys. Rev. B **71**, 033402 (2005).
- [20] F. Wang, G. Dukovic, L. E. Brus, and T. F. Heinz Phys. Rev. Lett. **92**, 177401 (2004).
- [21] O. J. Korovyanko, C.-X. Sheng, Z. V. Vardeny, A. B. Dalton, and R. H. Baughman Phys. Rev. Lett. **92**, 017403 (2004).
- [22] T. Hertel, A. Hagen, V. Talalaev, K. Arnold, F. Hennrich, M. Kappes, S. Rosenthal, J. McBride, H. Ulbricht, and E. Flahaut, Nano Lett. **5**, 511 (2005).
- [23] J. Feldmann *et al.*, Phys. Rev. Lett. **59**, 2337 (1987).
- [24] D. S. Citrin, Phys. Rev. Lett. **69**, 3393 (1992).
- [25] F. Stern, in *Solid State Physics*, edited by F. Seitz and D. Turnbull (Academic, NewYork, 1963), Vol. 15, Sec. 36.
- [26] R. Saito and H. Kataura, in *Carbon Nanotubes: Synthesis, Structure, Properties and Application*, edited by M. S. Dresselhaus, G. Dresselhaus, Ph. Avouris (Springer-Verlag, Heidelberg 2001), Vol. 80.
- [27] M. Rohlffing and S. G. Louie, Phys. Rev. B **62**, 4927 (2000).
- [28] E. Hanamura, Phys. Rev. B. **38**, 1228 (1988).
- [29] J. Gonzalez, F. Guinea, M. A. H. Vozmediano, Phys. Rev. B **59**, R2474 (1999); C. L. Kane and E. J. Mele, Phys. Rev. Lett. **93**, 197402 (2004).
- [30] V. Perebeinos, J. Tersoff, Ph. Avouris, Phys. Rev. Lett. **94**, 086802 (2005).